Science Advances

AAAS

advances.sciencemag.org/cgi/content/full/2/12/e1601530/DC1

Supplementary Materials for

Reactive nitrogen chemistry in aerosol water as a source of sulfate during haze events in China

Yafang Cheng, Guangjie Zheng, Chao Wei, Qing Mu, Bo Zheng, Zhibin Wang, Meng Gao, Qiang Zhang, Kebin He, Gregory Carmichael, Ulrich Pöschl, Hang Su

Published 21 December 2016, *Sci. Adv.* **2**, e1601530 (2016)
DOI: 10.1126/sciadv.1601530

This PDF file includes:

Supplementary Materials

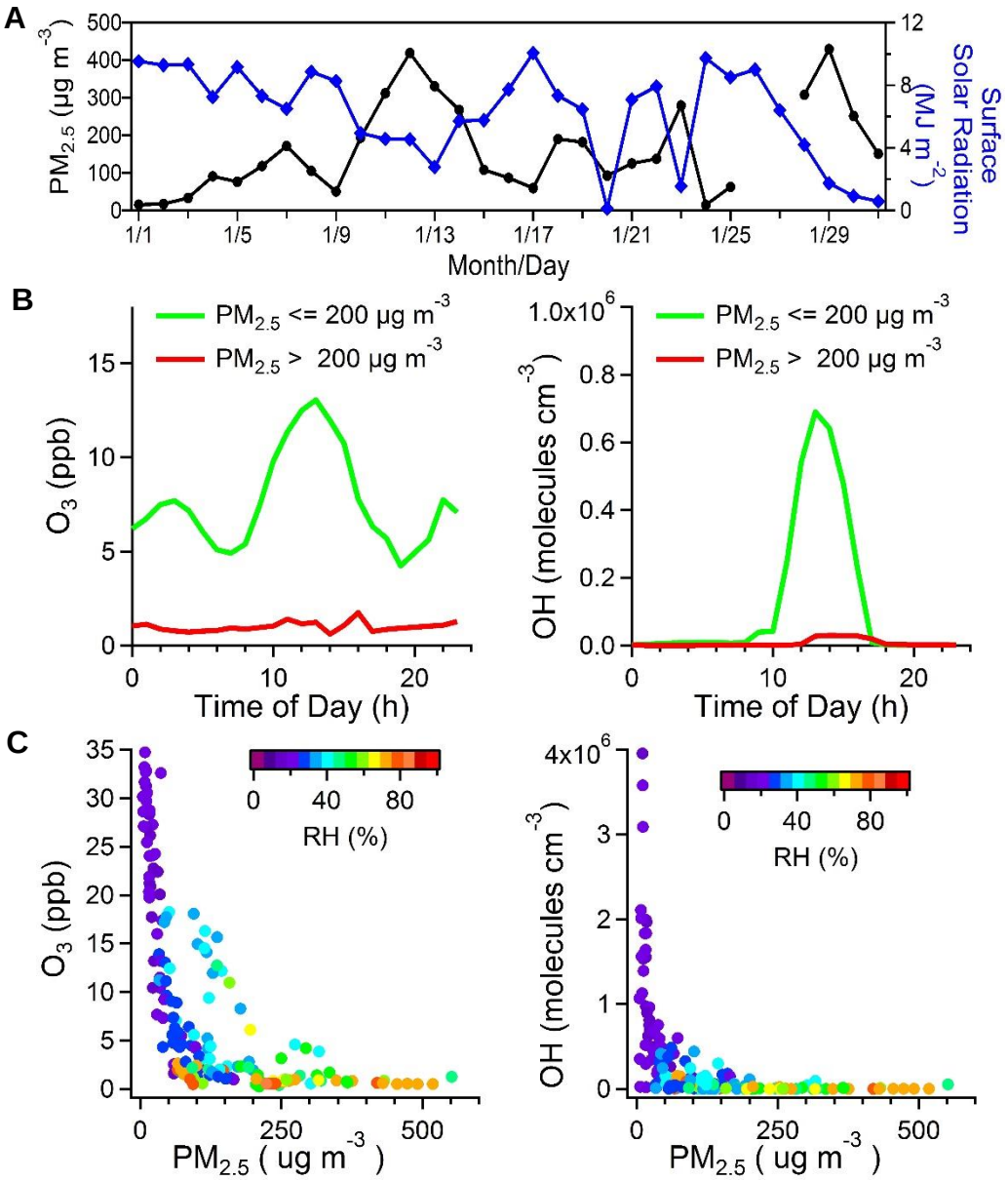

fig. S1. Weakened photochemistry by aerosol dimming effects during January 2013 in Beijing. (**A**) Relationship between the observed total surface solar radiation and ground based measurement of $PM_{2.5}$. (**B**) Diurnal pattern of observed O_3 and model simulated OH (*7*) for hours with $PM_{2.5} \leqslant 200\ \mu g\ m^{-3}$ and hours with $PM_{2.5} > 200\ \mu g\ m^{-3}$. (**C**) The observed O_3 and modeled OH (*7*) are plotted against the observed $PM_{2.5}$ concentration. Only midday (10:00–15:00 local time) data when photochemistry is expected to be the strongest of the day are shown.

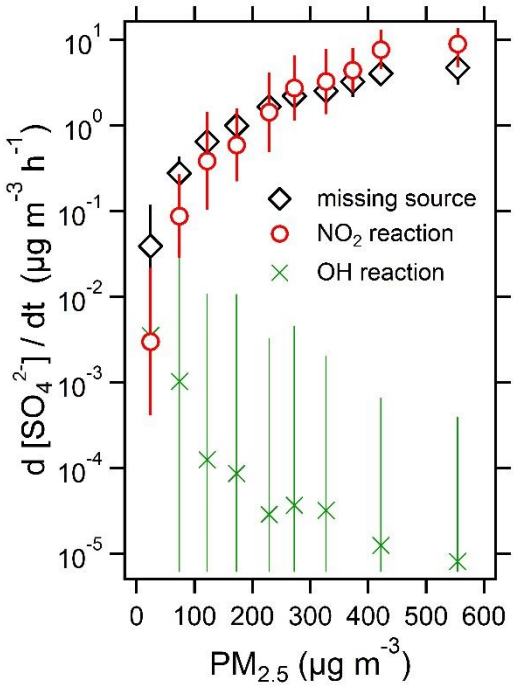

fig. S2. Importance of the NO_2 reaction pathway for sulfate production in the Beijing haze (January 2013). Sulfate production rates calculated for the aqueous phase NO_2 reaction pathway (red circles) and the gas phase OH reaction pathway (green crosses) compared to the missing source of sulfate (black diamonds) (geometric mean ± SD) (*5*, *7*). The pH of aerosol water here is calculated based on the observed size-segregated aerosol chemical composition (*70*) as shown in Fig. 1D ($PM_{1.1}$, diamond; $PM_{1.1\text{-}2.1}$, triangle).

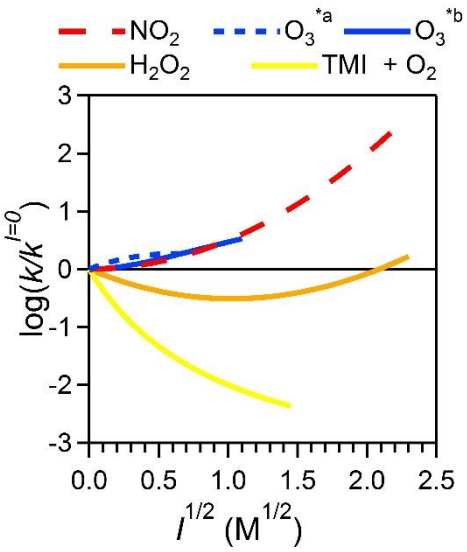

fig. S3. Influence of ionic strength (*I*) on rate of aqueous sulfate-producing reactions. $k^{I=0}$ indicates the kinetic constant at I = 0 M. Detailed expressions of k and the $\log(k/k^{I=0})$~I relationship are listed in table S7. O_3^{*a} and O_3^{*b} refer to the relationship suggested by Maahs *et al.* (*53*) and Lagrange *et al.* (*54*), respectively. More details can be found in section M8.

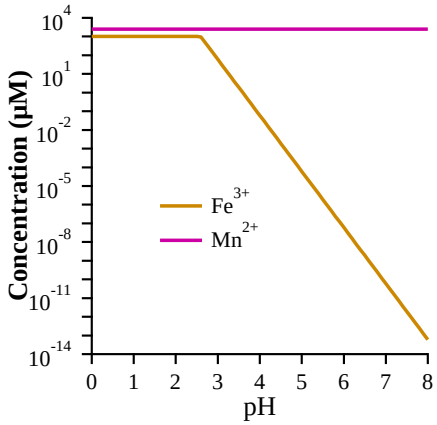

fig. S4. Estimation of Fe^{3+} and Mn^{2+} concentrations as a function of aerosol water pH during Beijing hazes. At higher pH, the solubility of $Fe(OH)_3$ and $Mn(OH)_2$ may become the limiting factor. The corresponding precipitation constant at 298K are 2.6×10^{-38} for $Fe(OH)_3$ and 1.6×10^{-13} for $Mn(OH)_2$ (*66*).

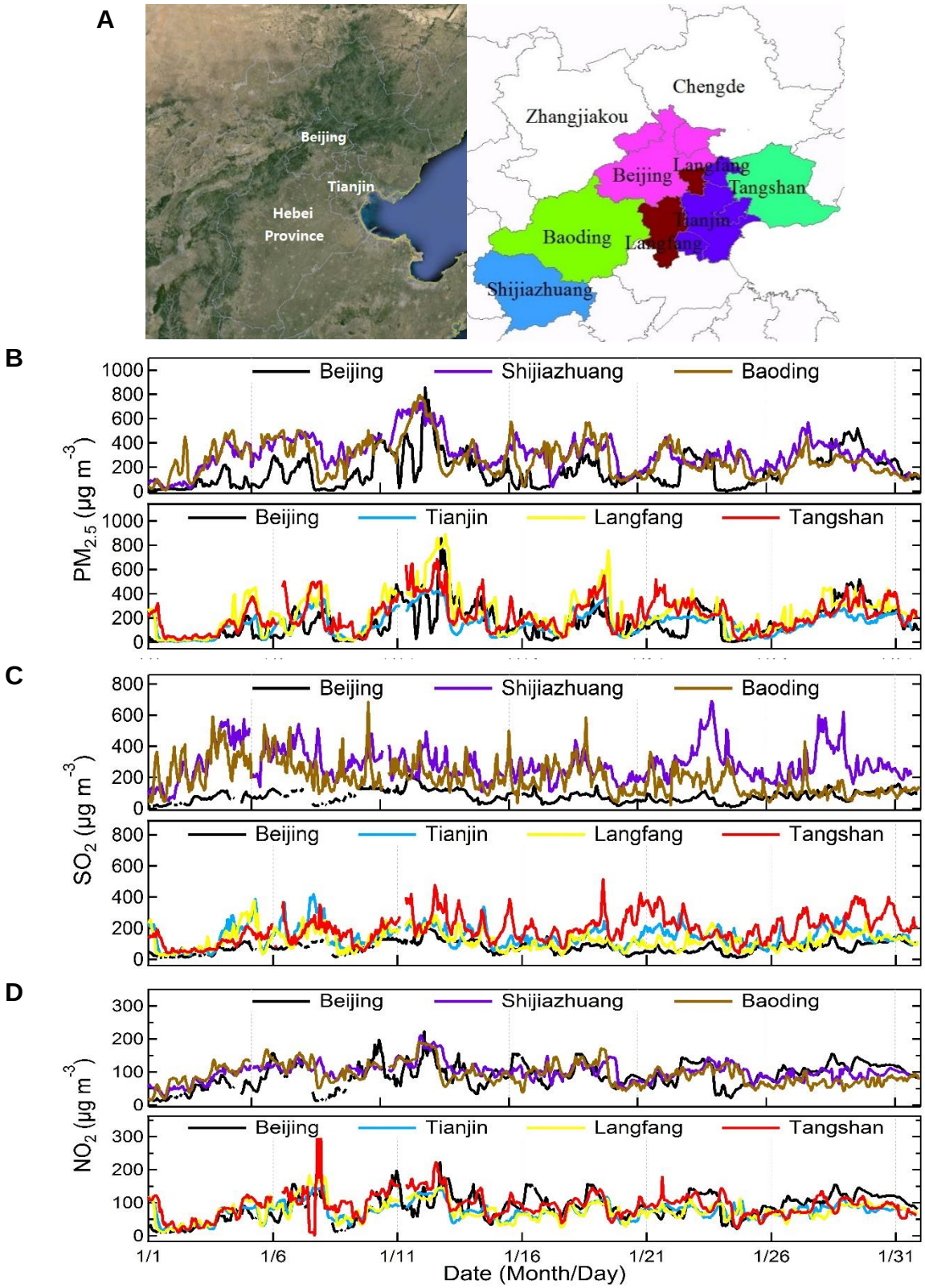

fig. S5. Regional pollution across the NCP during January 2013. (**A**) Topographic map around Beijing, and location of all cities shown below. (**B**) $PM_{2.5}$ (**C**) SO_2 and (**D**) NO_2 concentrations in Beijing and its southwest (upper panel) and southeast (lower panel) cities.

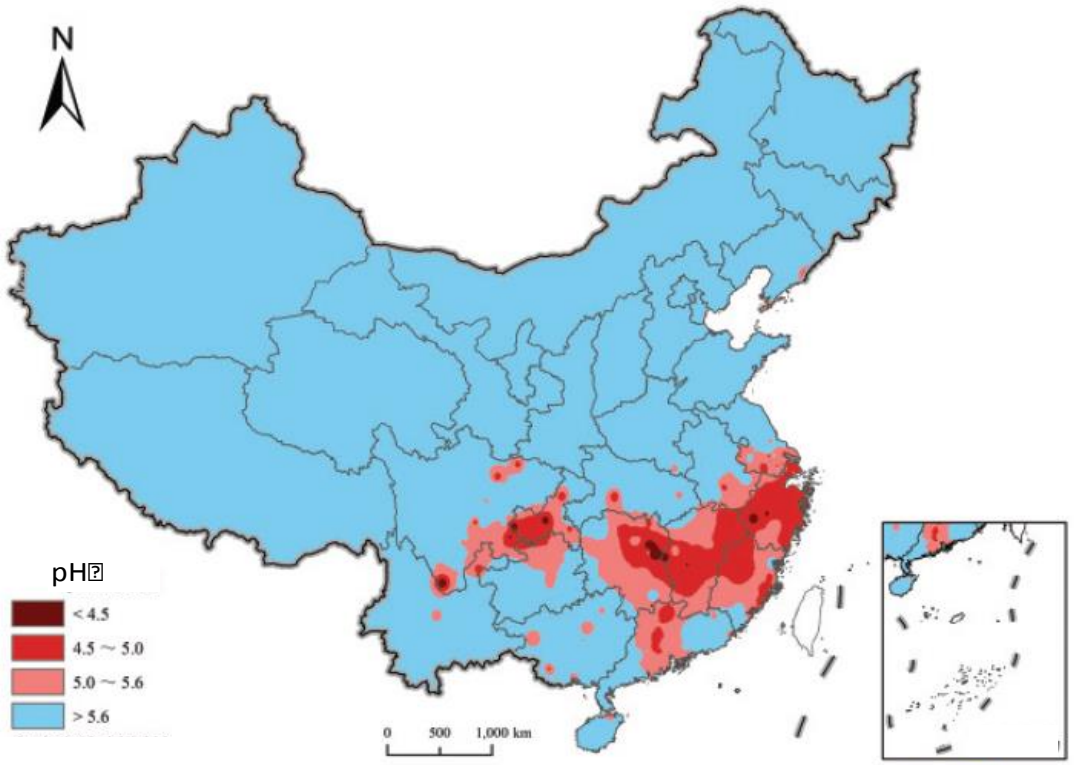

fig. S6. Annual precipitation pH of China in 2013. (source: Report of China's Environmental Quality in 2013, by Ministry of Environmental Protection of People's Republic of China, http://jcs.mep.gov.cn/hjzl/zkgb/).

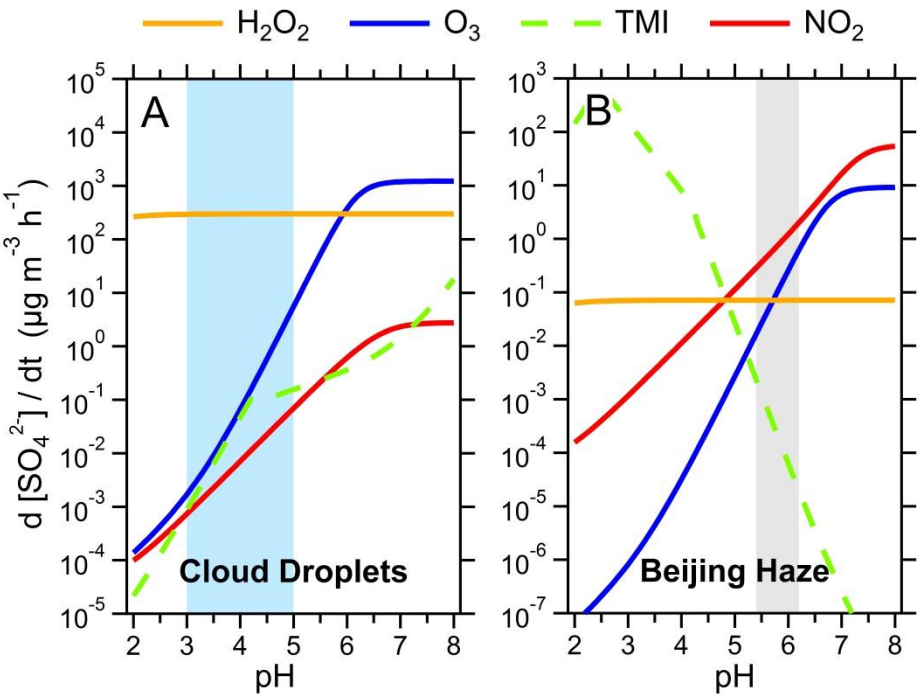

fig. S7. The same as Fig. 2 but with a lower limit of reaction rate constants reported by Lee and Schwartz (*18*).

table S1. Previously reported concentrations of cations and anions in $PM_{2.5}$ during winter for cities in NCP used in Fig. 1D.

City	Site Type	Year	Cations [b] ($\mu mol\ m^{-3}$)	Anions [b] ($\mu mol\ m^{-3}$)	Cations / Anions	Reference
Beijing	Urban	2009-2010	0.41	0.39	1.03	(*108*)
	Urban	2007	0.45	0.37	1.20	(*82*)
	Urban	2005-2006	0.84	0.66	1.28	(*109*)
	Rural	2005-2006	0.45	0.31	1.48	
		2003	1.20	1.10	1.09	(*22*)
	Urban	2002-2003	0.93	1.09	0.85	(*110*)
	Urban (Industrial)	2002-2003	0.96	0.88	1.09	
	Urban (Residential)	2002-2003	1.44	1.14	1.26	
Jinan	Urban	2007~2008	1.85	1.49	1.24	(*111*)
	Urban	2004~2005	1.66	1.39	1.20	(*83*)
Tianjin	Urban	2003	1.78	1.63	1.10	(*22*)
Qingdao	Urban	2003	1.53	1.32	1.16	(*22*)

[a] Only studies which have reported the seasonal-averaged concentrations of all major water-soluble inorganic ions (i.e. Na^+, K^+, Ca^{2+}, Mg^{2+}, NH_4^+, SO_4^{2-}, NO_3^- and Cl^-) are selected.

[b] Concentrations of cations and anions are estimated as

$$\text{Cations}\ (\mu mol\ m^{-3}) = \frac{[Na^+]}{23} + \frac{[K^+]}{39} + \frac{[Ca^{2+}]}{20} + \frac{[Mg^{2+}]}{12} + \frac{[NH_4^+]}{18}$$

$$\text{Anions}\ (\mu mol\ m^{-3}) = \frac{[Cl^-]}{35.5} + \frac{[SO_4^{2-}]}{48} + \frac{[NO_3^-]}{62}$$

table S2. Summary of field observation and methods in this study.

Species	Method	Time Resolution	Period
$PM_{2.5}$ and PM_{10}	PM-712 Monitor (Kimoto Electric Co., Ltd., Osaka, Japan)	1h	Jan. 1st to Jan. 31st
Meteorology data	Milos520 Weather Station (VAISALA Inc., Finland).	1h	Jan. 1st to Jan. 31st
OC and EC	Sunset model 4 semi-continuous carbon analyzer (Beaverton, OR, USA)	1h	Jan. 1st to Jan. 31st
SO_4^{2-} and NO_3^-	ACSA-08 Monitor (Kimoto Electric Co., Ltd., Osaka, Japan)	1h	Jan. 1st to Jan. 31st
Water-Soluble Inorganic Ions[a]	Offline Sampling - Ion Chromatograph analysis	2h	Jan. 12th to Jan. 24th
Water-Soluble Inorganic Ions[a]	Offline Sampling - Ion Chromatograph analysis	24h	Jan. 1st to Jan. 31st

[a] Including Na^+, K^+, Ca^{2+}, Mg^{2+}, NH_4^+, SO_4^{2-}, NO_3^- and Cl^-.

table S3. Domain, configurations, and major dynamic and physical options used in WRF v3.5.1. (Source: Zheng et al. (*7*)).

Simulation period	**Dec 2012 and Jan 2013**
Domain	East Asia (columns: 178, rows: 133) with three extra grids in each boundary of Domain 1 (columns: 172, rows: 127)
Horizontal resolution	36 km
Vertical resolution	23 sigma levels from surface to tropopause (about 100 mb)
Meteorological IC and BC	Reanalysis data from the National Centers for Environmental Prediction Final Analysis (NCEP-FNL)
Shortwave radiation	New Goddard scheme (*112*)
Longwave radiation	The rapid radiative transfer model (RRTM) (*113*)
Land surface model	The USGS 24-category land use data
Surface layer	Pleim–Xiu land surface scheme (*114*)
Planetary boundary layer model	ACM2 PBL scheme (*115*)
Cumulus parameterization	Kain–Fritsch cumulus scheme (*116*)
Cloud microphysics	WSM6 (*117*)
Analysis nudging	Temperature and water vapor mixing (above PBL); wind (in and above PBL)
Observational nudging	Temperature, water vapor mixing and wind (in and above PBL)
Soil nudging	Include soil moisture and temperature
FDDA data	NCEP Automated Data Processing (ADP) surface (ds461.0) and upper (ds351.0) air data

table S4. Rate expression and rate coefficients of relevant aqueous-phase reactions.

Oxidants	Rate Expression, -d[S(IV)]/dt	Reference
O_3	$(k_0[SO_2\cdot H_2O]+k_1[HSO_3^-]+k_2[SO_3^{2-}])[O_3(aq)]$ $k_0 = 2.4\times10^4\ M^{-1}s^{-1}$ $k_1 = 3.7\times10^5\ M^{-1}s^{-1}$, E/R= 5530 K[a] $k_2 = 1.5\times10^9\ M^{-1}s^{-1}$, E/R= 5280 K	(*12*)
H_2O_2	$(k_3[H^+][HSO_3^-][H_2O_2(aq)])/(1+K[H^+])$ $k_3 = 7.45\times10^7\ M^{-1}s^{-1}$, E/R= 4430 K $K = 13\ M^{-1}$	(*12*)
TMI+O_2, where TMI are Fe(III) and Mn(II)[b]	$pH \le 4.2$, $k_4[H^+]^{-0.74}[Mn(II)]Fe(III)][S(IV)]$ $k_4 = 3.72\times10^7\ M^{-1}s^{-1}$ $pH > 4.2$, $k_5[H^+]^{0.67}[Mn(II)]Fe(III)][S(IV)]$ $k_5 = 2.51\times10^{13}\ M^{-1}s^{-1}$	(*118*)
NO_2 [e]	$k_6[NO_2(aq)][S(IV)]$ $k_{6,\,low}$ [c] = (0.14~2) $\times10^6\ M^{-1}s^{-1}$, E/R= 0 K $k_{6,\,high}$ [d] = (1.24 ~1.67) $\times10^7\ M^{-1}s^{-1}$	*(12, 18, 61)*
MHP (methyl-hydrogen peroxide)	$k_7[H^+][HSO_3^-][MHP(aq)]$ $k_7 = 1.75\times10^7\ M^{-1}s^{-1}$, E/R= 3801 K	(*20*)
PAA (peroxyacetic acid)	$(k_8[HSO_3^-][PAA(aq)])/([H^+]+K_8)$ $k_8 = 3.64\times10^7\ M^{-1}s^{-1}$, E/R= 3994 K $K_8 = 1.65\times10^{-5}$ M	(*20*)

[a] According to the Arrhenius equation, the dependence of kinetic constant *k* on temperature T could be expressed as

$$k(T) = k(T_0)\exp\left[-\frac{E}{R}\left(\frac{1}{T}-\frac{1}{T_0}\right)\right] \text{ where } T_0 = 298\ K.$$

[b] Only Fe(III) and Mn(II) are considered here, since other transition metal ions (TMIs), such as Sc(III), Ti(III), V(III), Cr(III), Co(II), Ni(II), Cu(II) and Zn(II), showed much less catalytic activities (*58*). In addition, it has been concluded that the decreased temperature would generally lead to a decrease in overall reaction rate, due to the effect that higher activation energy would overweigh the increased SO_2 solubility (*12*). Due to the lack of information on E/R, we used both kinetic and SO_2 solubility at 298K, which would be an overestimation in Beijing haze scenario (271K) for the sulfate production rate by TMIs reaction pathway.

[c] The lower estimate of k_6 ($k_{6,\,low}$) are derived from Lee and Schwartz (*18*). They determined a $k_6 = 1.4\times10^5\ M^{-1}s^{-1}$ at pH 5.0, but only a lower limit of $2\times10^6\ M^{-1}s^{-1}$ at pH 5.8 and 6.4. Thus we used a stepwise function with pH for estimation of $k_{6,\,low}$. When pH < 5, $k_{6,\,low} = 1.4\times10^5\ M^{-1}s^{-1}$, while for pH>5.8, $k_{6,\,low} = 2\times10^6\ M^{-1}s^{-1}$, and for pH between 5 and 5.8 the linear interpolated values are used.

[d] Clifton et al. (*61*) suggested a 10~100 times higher value than Lee and Schwartz (*18*), and their results are used as the higher estimation of k_6 ($k_{6,\,high}$). Similarly, their reported pH-dependence was taken into consideration with a stepwise function. At pH 5.3 and 8.7 (which is already beyond our interested pH range), $k_{6,\,high}$ are respectively 1.24×10^7 and $1.67\times10^7\ M^{-1}s^{-1}$, and at pH 5.3~8.7 the linear interpolated values are used.

[e] In Fig. 2, the average rate calculated by $k_{6,\,low}$ and $k_{6,\,high}$ are used.

table S5. Constants for calculating the apparent Henry's constant (*H)[a].**

Gas-Aqueous Equilibrium for S(IV)			
Equilibrium	Constant Symbol	H_{298K} (M atm^{-1})[b]	$-\triangle H_{298K}/R$ (K)
$SO_2(g) \leftrightarrow SO_2(aq)$	H_{SO2}	1.23	3145.3
$O_3(g) \leftrightarrow O_3(aq)$	H_{O3}	1.1 (-2)	2536.4
$H_2O_2(g) \leftrightarrow H_2O_2(aq)$	H_{H2O2}	1.0 (5)	7297.1
$NO_2(g) \leftrightarrow NO_2(aq)$	H_{NO2}	1.0 (-2)	2516.2
Aqueous-phase Ionization Equilibrium[c]			
Equilibrium	Constant Symbol	K_{298K} (M)[b]	$-\triangle H_{298K}/R$ (K)
$SO_2 \cdot H_2O \leftrightarrow H^+ + HSO_3^-$	K_{s1}	1.3 (-2)	1960
$HSO_3^- \leftrightarrow H^+ + SO_3^{2-}$	K_{s2}	6.6 (-8)	1500

[a] Read 1.0 (5) as 1.0×10^5. Data are extracted from Chapter 7 of Ref. (*12*).

[b] The Henry's constant (H) and ionization constant (K) are both equilibrium constant in nature, and thus have the same dependence on temperature. The H at temperature T is

$$H(T) = H(T_0)\exp\left[-\frac{\Delta H_{298K}}{R}\left(\frac{1}{T}-\frac{1}{T_0}\right)\right]$$

where T_0 = 298 K. The same is true for K(T).

[c] The effective Henry's constant (H*) for HSO_3^-, SO_3^{2-} and S(IV) (which is defined as sum of $[SO_2 \cdot H_2O]$, $[HSO_3^-]$ and $[SO_3^{2-}]$) are respectively

$$H^*_{HSO_3^-} = H_{so_2}\frac{K_{s1}}{[H^+]}$$

$$H^*_{SO_3^{2-}} = H_{so_2}\frac{K_{s1}K_{s2}}{[H^+]^2}$$

$$H^*_{S(IV)} = H_{so_2}[1+\frac{K_{s1}}{[H^+]}+\frac{K_{s1}K_{s2}}{[H^+]^2}]$$

where H_{SO2}, K_{s1} and K_{s2} are corresponding values at temperature T.

table S6. Summary of suggested activity coefficient (*a*)–ionic strength (*I*) dependence[b].

Equation Name	Equation	Targeted Species	Upper Valid Limit of I (M)	Reference
Debye-Hückel	$\log a_i = -Az_i^2\sqrt{I}$	Ions	~ 0.01	(*119*)
Setschenow[b]	$\log a_i = bI$	Neutral species	~5[b]	(*120*)
Simple extended Debye-Hückel	$\log a_i = -Az_i^2\frac{\sqrt{I}}{1+\sqrt{I}}$	Ions	~ 0.1	(*121*)
Davies	$\log a_i = -Az_i^2(\frac{\sqrt{I}}{1+\sqrt{I}} - 0.3I)$	Ions	~ 0.7	(*121*)
Extended Debye-Hückel ("B-dot" equation)	$\log a_i = -Az_i^2\frac{\sqrt{I}}{1+Ba_i^\circ\sqrt{I}} + bI$	Ions and neutral species	~1	(*122*)
Pitzer	$\log a_i = \log a_i^{LR} + \log a_i^{MR} + \log a_i^{SR}$ [c]	Ions and neutral species	>1	(*123*, *124*)

[a] Notation of the common symbols: a_i and z_i are respectively the activity coefficient and charge number of ion *i*, *I* is the ionic strength, others are constants.

[b] The Setschenow equation was at first intended to describe the pattern of changed solubility with electrolyte concentration, and Debye and McAulay (*120*) provided an theoretical explanation for this equation. The valid range may change with solute and solvent; but it was generally valid when $I < 5$ M (e.g., (*125–127*)).

[c] The LR, MR and SR refer to Long-, Middle- and Short-Range effects, respectively. See the most recently studies in Rusumdar (*128*).

table S7. Influence of ionic strength (*I*) on rate of aqueous sulfate-producing reactions.

Oxidants	Rate Expression, -d[S(IV)]/dt	Relation of $k/k^{I=0}$ with Ionic Strength I[a]	Condition Notes	Reference
H_2O_2	$k_1[H^+][HSO_3^-][H_2O_2(aq)]$	$\log\frac{k}{k^{I=0}} = -\frac{2A\sqrt{I}}{1+B\sqrt{I}} + 2\beta I$ A=0.509 $M^{-0.5}$, B=0.17 $M^{-0.5}$, β=0.18 M^{-1}	I_{max} = 5 M; *a-I* Type: Pitzer	(*52*) and references therein
O_3[b]	$k_2[S(IV)][O_3(aq)]$; $k_2 = k_{2A}+k_{2B}[OH^-]$	$\log\frac{k}{k^{I=0}} = b_2(\frac{\sqrt{I}}{1+\sqrt{I}} - 0.3I)$ b_2=1.0 (ranges 0.7 to 1.3)[b]	I_{max} = 0.4 M; pH = 3~6.2 *a-I* Type: Davies	(*53*)
	$k_3[HSO_3^-][O_3(aq)][H^+]^{-0.5}$	$\frac{k}{k^{I=0}} = 1 + b_3 I$ b_3=1.94 M^{-1} (ranges 1.34 to 6.13)[b]	I_{max} = 1.2M	(*54*)
$TMI+O_2$[c]	$k_4[S(IV)][TMI][H^+]^{-1}$; TMI = Fe(III) or Mn(II)	$\log\frac{k}{k^{I=0}} = b_4\frac{\sqrt{I}}{1+\sqrt{I}}$ b_4= -4 (ranges -2 to -4)[c]	I_{max} = 2 M; pH = 3.0 *a-I* Type: Extended Debye-Hückel	(*55*, *56*)
NO_2[d]	$k_5[S(IV)][NO_2(aq)]$	$\log\frac{k}{k^{I=0}} = b_5 I$ b_5=0.5 M^{-1} [d]	*a-I* Type: Setschenow	/

[a] All ionic strength *I* in the expressions are with the unit of M.

[b] Different values of *b* are reported with changing solution chemical environments, while the general form are kept (*53*, *54*). Here we used a medium value of b_2=1.0 and b_3=1.94, respectively, to show the general pattern.

[c] b_4 are -2 for Fe(III) and -4 for Mn(II). In fact, this expression was insufficient to fully predict the sulfate inhibition effect. As a result, here the value of -4 are used to better represent the situation (*55*, *56*).

[d] Value of b_5 are not reported, but is only our theoretical prediction. The value of 0.5 was assumed to show the trend. Note that a positive value is implied in its definition.